



**HAL**  
open science

## Shape and roughness extraction of line gratings by small angle X-ray scattering: statistics and simulations

Jérôme Reche, Patrice Gergaud, Yoann Blancquaert, Maxime Besacier,  
Guillaume Freychet

### ► To cite this version:

Jérôme Reche, Patrice Gergaud, Yoann Blancquaert, Maxime Besacier, Guillaume Freychet. Shape and roughness extraction of line gratings by small angle X-ray scattering: statistics and simulations. IEEE Transactions on Semiconductor Manufacturing, 2022, 35 (3), pp.425 - 431. 10.1109/TSM.2022.3176026 . cea-04249757

**HAL Id: cea-04249757**

**<https://cea.hal.science/cea-04249757v1>**

Submitted on 19 Oct 2023

**HAL** is a multi-disciplinary open access archive for the deposit and dissemination of scientific research documents, whether they are published or not. The documents may come from teaching and research institutions in France or abroad, or from public or private research centers.

L'archive ouverte pluridisciplinaire **HAL**, est destinée au dépôt et à la diffusion de documents scientifiques de niveau recherche, publiés ou non, émanant des établissements d'enseignement et de recherche français ou étrangers, des laboratoires publics ou privés.

# Shape and Roughness Extraction of Line Gratings by Small Angle X-Ray Scattering : Statistics and Simulations

Jérôme RECHE, Patrice GERGAUD, Yoann BLANCQUAERT, Maxime BESACIER, Guillaume FREYCHET

**Abstract**— Since 2010, a lot of progress was done concerning Small Angle X-ray Scattering (SAXS) extraction capabilities for dimensional control of line gratings [1]–[3]. Firstly, experimental methodologies to extract the pitch, the critical dimension (CD) and the side-wall angle (SWA) of line gratings were developed. Secondly, line roughness was measured and we demonstrated that the SAXS technique has the sensitivity to measure line roughness amplitude below 1 nm on a set of designed gratings [4]. Thirdly, thanks to Fast Fourier Transform (FFT) simulations, we determined that the Line Width Roughness (LWR) defined as a Power Spectral Density (PSD) can be measured in a SAXS pattern [5]. This led to a comparison between the LWR PSD extracted on one set of sample by both SAXS and Scanning Electron Microscopy (SEM) [6]. In this new paper, we extend the description and discussion of the methodology to extract information from SAXS started on our previous study. A new set of samples was designed and measured at a new beamline configuration with higher angular resolution. Moreover, we study count statistic to determined last roughness parameter with simulation real diffraction comparison.

**Index Terms**— SAXS, metrology, Line Roughness, PSD, dimensional control

## I. INTRODUCTION

Concomitantly to the development of microelectronics needs (Internet of Things, big data, artificial intelligence), devices produced by the microelectronics industry must be smaller and more performant. This implies to improve continuously fabrication processes, with breakthroughs in the architectures of the systems. One of the key points is to overcome the reduction of energy consumption by devices. Such a reduction is strongly related to a reliable control of the morphology of line gratings constituting the device. The fabrication of such nanostructures requires new tools to characterize their shapes, sizes and defects. In fact, the continuous minimization of nanostructure sizes pushes conventional techniques, such as SEM or atomic force microscopy (AFM), to their limits. Transmission-SAXS (T-

SAXS) and Grazing Incidence-SAXS (GI-SAXS) are characterization techniques considered promising for dimensional control by the International Roadmap for Devices and Systems (IRDS) [3].

This study focuses on T-SAXS measurements and associated methodologies to reconstruct the shape of line gratings and extract the lateral line roughness. The setups, software and samples used in this study will be described in the section II, followed by the explanation of the SAXS methodology for shape reconstruction and roughness extraction in section 3. Finally, the information extracted from SAXS results applied on a new set of samples is compared with both TEM and forward simulations, respectively for shape validation and roughness explanation.

## II. TOOLS AND SAMPLES

Since more than 15 years, the design and fabrication of line gratings with controlled periodic roughness have been used for the development of roughness extraction methodologies for SEM, AFM and scatterometry [7], [8] as well as for SAXS [4], [9]. Nevertheless, the specific case of periodic roughness is not representative of the roughness generated during the device fabrication. Previous study [ASMC] presents a new approach to mimic the roughness coming from the device process. In this study we go further with use of an adapted synchrotron beamline and specific methodology and compare results with simulations.

### A. X-Ray Setup and acquisition

Critical-Dimension SAXS (CD-SAXS) experiments were performed at the Soft Matter Interfaces Beamline (SMI, Beamline 12-ID) at the National Synchrotron Light Source II. A photon energy of 16.1keV was used with a beam size of  $250 \times 25 \mu\text{m}^2$  (HxV) at the sample position. Scattered intensity was recorded with Pilatus3 1M which is positioned at 8.29 meters from the sample.

The samples were positioned on top of x, y and z translation

J. RECHE, P. GERGAUD and Y. BLANCQUAERT are with Univ. Grenoble Alpes, CEA, Leti, 38000 Grenoble, France. (contact author: jerome.reche@cea.fr)

M. BESACIER is with Univ. Grenoble Alpes, CNRS, LTM 38000 Grenoble, France.

G. FREYCHET is with NSLSII, Brookhaven National Laboratory, Brookhaven, NY, USA

stages and an azimuthal rotation for an accurate alignment. As depicted in Fig. 1, the incident beam propagates along the z direction, normal to the surface of the sample when  $\omega$  is equal to 0 degree. Therefore, at  $\omega$  equal to 0, the sample is oriented along the (x, y) plane, and the CD-SAXS image is recorded in the  $(q_x, q_y)$  reciprocal space map.  $q_x$  and  $q_y$  are the components of the wave vector transfer  $q$  related to the in-plane angle  $2\theta_f$  and out-of-plane angle  $\alpha_f$  annotated on Fig. 1. The azimuthal angle  $\omega$  allows the rotation of the sample around the y-axis in order to access to the  $q_z$  direction of the reciprocal space. By measuring CD-SAXS images at several  $\omega$  positions a  $(q_x, q_z)$  reciprocal space map (RSM) is reconstructed .

In comparison to the beamline used in our previous study, the greater sample to detector distance available and lower beam divergence improved the resolution of the Bragg peaks recorded on the scattering image. As illustrated on Fig. 2a, the first peak is visible and each order is defined on 5x5pixels, increasing the quality of future peak fitting. Besides, the automated translation of the detector enabled image scattering acquisition at two detector positions, with a translation along y displacement, to build, as visible in Fig. 2b, an image without vertical detector gap. Finally, background measurements were done on the neighboring silicon substrate, gratings free, to remove noise and acquisition artifacts such as the truncation rods visible in Fig. 2b arising from the Si substrate.

### B. Software

In this study we used two kinds of software. The first one is dedicated to shape fitting through an inverse algorithm. It is based on the CD-SAXS plugin of Xi-Cam software [10] modify with custom-made python implementation. This software visualize grating as a x,z line profile and the parametrization is done through a stack of trapezoids. The data are fitted with an inverse algorithm.

The second software, in python too, generate binary image of a sample in (x, y) plan. This virtual sample represents the top-view of several lines and includes line roughness defined by a Power Spectral Density (PSD) model [11]. The second software also performed diffraction calculation based on the binary image generated through the square of the absolute value of the 2D Fast Fourier Transform (FFT) assuming a Fraunhofer diffraction configuration. An example of sample and diffraction obtained is visible in Fig. 3.

### C. Samples Preparation

The different samples studied in this paper contained line gratings with pitches of 100 nm and 113 nm without any specified roughness. They have been prepared using 193i lithography with different dose to obtain different CD and roughness. Final samples are obtained in silicon after etching and stripping steps.

As one can see on the TEM cross-section, Fig. 4, which could be consider as reference for 3D shape, the pattern is not perfectly rectangular. More exactly a footing (i.e. round part at bottom of line) is visible and due to the etching of the unused underlayer.

## III. THE DIFFERENT STAGES OF RSM ANALYSIS

The first step of the analysis is to determine the pitch of the line gratings.

### A. Pitch Extraction

In order to obtain the pitch, a CD-SAXS image at  $\omega$  equal 0 degree is acquired. The real space image is then converted to the  $(q_x, q_y)$  plane of the reciprocal space, as illustrated on Fig. 5. Afterwards, a one-dimensional cut along  $q_x$  at  $q_y = 0 \text{ nm}^{-1}$  was done. This cut intercepts the different Bragg peaks of the line gratings. The Fig. 6 shows the position of each Bragg peak along  $q_x$  as a function of peak index. These data were fitted using a linear model that follows the equation:

$$q_{x,n} = \frac{2\pi n}{L} \quad (1)$$

where  $q_{x,n}$  is the position along  $q_x$  of the  $n^{\text{th}}$  peak and  $L$  is the pitch of the gratings. In Fig. 6 a pitch of 113.16 nm is extracted, in agreement with the nominal value of 113 nm. After extracting the pitch, we proceed to the line shape extraction.

### B. 3D Profile of Lines

As shown previously, the 2D image taken at  $\omega=0^\circ$  gives only a  $(q_x, q_y)$  Reciprocal Space Map (RSM). As a consequence, this configuration allows probing the CD of the lines, averaged over the whole line height, i.e. the z-direction [12]. Therefore, it is impossible in this configuration to extract the information about the 2-dimensional structure of the silicon lines and spaces. To obtain such information, we used the methodology developed by Sunday et al. [3]. It consists in rotating the gratings to probe the  $q_z$  direction of the reciprocal space. For each angle  $\omega$ , the  $q$  value obtained along the x axis, can be projected in the  $q_x$  and  $q_z$  planes as:

$$\begin{cases} q_x = q \cos \omega \\ q_z = q \sin \omega \end{cases} \quad (2)$$

A final  $(q_x, q_z)$  map is obtained as shown in Fig. 7 after collecting 2D images from -60 to 60 degrees with 1 degree step and an acquisition time of xx s per image This representation of the reciprocal space helps to visualize the intensity variation of each Bragg peak versus  $\omega$ . Indeed, the modulation along the vertical rods observed on Fig. 7 comes directly from the in-depth profile of the line, also known as form factor, and corresponds to the in-depth line profile Fourier transform.

One-dimensional cuts along  $q_z$  at the  $q_x$  position of the five first lattice peaks were done. Intensity variations observed can be attributed to the form factor of the line profile. The intensity profiles along  $q_z$  were fitted using an inverse algorithm, namely a genetic algorithm, using on a Monte Carlo– Markov Chain methodology. The approach consists in minimizing the difference between a simulated model and the experimental data [2], [13]. An example of fitted data is given in Fig. 8 and the associated line profile on Fig. 9. In this approach, the line profile was defined as a stack of n trapezoids. Each trapezoid was described with a bottom CD, a height (kept similar for each trapezoid of the stack) and a sidewall angle. The computing time was optimized by using analytic expression to calculate efficiently the Fourier transform of the trapezoid stack and

itearet over numerous trapezoidal shape combinations.

### C. PSD Extraction Methodology

In 2019, we demonstrated for the first time the PSD LWR extraction from simulated T-SAXS data [5]. These simulations showed that the contribution of different roughness can be obtained in x-ray scattering patterns along the  $q_y$  axis (equivalent to the off specular case of X-ray reflectivity).

This is illustrated on Fig. 10a-d. In Fig. 10a, a perfect array of line without roughness gave a scattering pattern in the  $q_x$  directions only. The introduction of roughness along the line leads to an increase of the scattering along  $q_y$ . Moreover, distinctive scattering patterns appeared when varying the roughness (with edges more or less correlated). The simulated roughness on Fig. 10.c corresponds to correlated edge roughness, where the LWR, variation of CD along the line, is equal to 0. Therefore, the roughness corresponds to pure Line Edge Roughness (LER), variation in position of an edge compared to a straight reference. Some areas of the scattering patterns along  $q_y$  shows complete extinction area, corresponding to a form factor extinction, following:

$$\sin\left(q_x \frac{CD}{2}\right) / \sin(q_x) = 0 \quad (3)$$

Solving (3), leads to the generic equation to calculate the position along  $q_x$  of the extinction:

$$q_x = \frac{(2k+1)\pi}{cd}, k \in \mathbb{Z} \quad (4)$$

where CD is the mean width of lines studied.

For anti-correlated edges (Fig. 10b), as for the uncorrelated edges case (Fig. 10d) minima can still be detected but without complete extinction at the positions mentioned previously. This leads to consider that the photons scattered at these specific  $q_x$  positions are only due to LWR. The Fraunhofer diffraction is well described by the square of a FFT and the Wiener-Khinchin theorem links the square of a FFT with the PSD. Therefore, the PSD of a LWR signal can be extracted from cuts along the  $q_y$  axis at some specific  $q_x$  positions. This methodology, was already validated with dedicated sample with known roughness [5], and compare to CD-SEM PSD extraction [6].

## IV. RESULTS AND DISCUSSIONS

T-SAXS acquisitions were done on 36 samples and the methodology described in the previous sections was applied for each sample. In the following, we will discuss the reliability of the extraction for the main parameters defined previously.

### A. Reliability of pitch analysis

In these different samples, two pitch families are presents, 100 nm and 113 nm. Results obtained are shown on Tab. 1. One can see that extracted pitches are close to target with bias below 0.2%. Moreover, the variation from sample to sample, which is below sub-angstrom, shows the good manufacturing and measurement reproducibility. Nevertheless, we detect that the pitched extracted with T-SAXS are always above the target, this

could come from a bias during the manufacture or an offset in the T-SAXS setup, possibly one is the sample to detector distance.

Target (nm)	Mean measure (nm)	STD (nm)
100	100.12	0.04
113	113.20	0.05

Tab. 1 : Pitch extraction with T-SAXS and comparison to target value.

### B. Reliability of shape extraction role of number of trapezoids

As illustrated on Fig. 11, the resolution of the reconstructed shape depends at the first order on the number of trapezoids used to define the line profile. High number of trapezoids allows accessing complex shapes, as visible with line-rounded foot on Fig. 11 which obviously cannot be described with only 1 trapezoid. Nevertheless, as the number trapezoids is increased, for example up to 16, the calculation becomes time consuming and lead oversampling phenomenon such as a noisy shape, as illustrated on Fig. 11 with the bump in the line feet. In opposition, the use of only few trapezoids leads to miss some information and converge towards ambiguous profile, as for example with 1 trapezoid case for “1-113-G” sample which gives an height around 7 nm lower than the expected nominal value., A compromise must therefore be found between extraction time, resolution obtained and residual error of the model. The residual error between the experimental data and the simulation with different number of trapezoids was calculated and reported in the Fig. 12. This figure highlights the importance of running the simulations with different number of trapezoids and optimize the simulated model to keep the residual error low and therefore improve the confidence in the final extracted model. It must be noticed that the number of optimum trapezoids can change from a structure to another and is dependent of structure complexity (i.e. slope break).

### C. Reliability of LWR PSD extraction, role of acquisition time

For this study, vertical cuts have been performed on the  $(q_x, q_y)$  RSM shown in the Fig. 5 at first extinction  $q_x = \pm 0.0759 \text{ nm}^{-1}$  along positive and negative value of  $q_y$ . The combination of these four extractions enable to cover a larger range of  $k_n$  and avoid some remaining acquisition artifacts. As a reminder, this methodology does not allow the extraction of the absolute level of the PSD (related to RMS amplitude), but the PSD profile gives information on  $\xi$ , the roughness correlation length or  $\alpha$  the Hurst parameter [14].

It is clearly visible in the Fig. 13 that the PSD obtained with 200 seconds acquisition is smoother than the ones obtained with shorter exposure time. Increase the exposure time enables to increase the number of photons collected on the detector and therefore to improve the signal to noise ration. This directly leads to cover a larger  $k_n$  range. As visible in Fig. 13, for 10s acquisition, it is tricky to analyze the PSD above  $0.1 \text{ nm}^{-1}$  due to the noisiness of the data. In opposite, with 200s there is also noise close to  $k_n = 1 \text{ nm}^{-1}$  but the trend of the curve is clearly observable . For 200s acquisition, the roughness parameters

extracted on the samples are  $\alpha = 0.463$  and  $\xi = 26.36$  nm. From our set of samples we tried to define the optimal exposure time required to extract the different roughness parameters. Fig. 14 shows that the extraction of the different parameters follows different trends with the parameter  $\xi$ , which can be obtained with 2s acquisition time while the parameter  $\alpha$  fluctuates until 150s acquisition time. Concerning the parameter  $\sigma$  more information about the number of incoming photons and about the total surface illuminated is needed to extract the absolute value with this method.

#### D. Complete PSD extraction methodology

As mentioned previously, the parameter  $\sigma$  (roughness amplitude) has not been determined experimentally. Thanks to all the parameters extracted before: pitch, CD, roughness parameters  $\alpha$  and  $\xi$ , simulations can be performed and adjusted to the experimental data. For that, the absolute intensity of the incident x-ray beam have been determined by calibrating the intensity on the first experimental Bragg peak, normalizing so the simulated data.

20 simulated images of samples with 20 lines for each have been built and diffraction patterns generated by calculating the Fourier transform of the created samples/images. The PSD extracted from each simulation are then averaged inducing a noise equivalent to the counting statistic. The averaged PSD curve is fitted using the PSD equation given in [ref => your PhD], providing a set of  $(\sigma, \xi, \alpha)$  parameters.. As an illustration, a sample roughness close to 3.2 nm is reported on Fig. 15. More precisely for a given  $q_x$  position, PSD fit of the experimental data gives  $\sigma_{\text{output}} = 0.656$  nm while the simulation gives  $\sigma_{\text{output}} = 0.644$  nm. A better extraction could be performed with dedicated roughness model, which we have not implemented yet.

### V. CONCLUSION

In this paper, we summarized the general methodology to extract the line shape and roughness in line gratings. We described step by step the full methodology to extract the pitch, CD, line shape and PSD of line gratings.

In order to establish the reliability of the data extraction by T-SAXS, a new set of samples was studied. We first presented the x-ray beamline configuration used for this study as well as the numerical tools used in this study.

We showed the high consistency in pitch extraction with sub-angstrom standard deviation. We also demonstrated that the number of trapezoids stacked to describe the line profile needs to be balanced between a fine description of the line shape and the accuracy and confidence in the resulting fit. This was demonstrated by comparing T-SAXS reconstruction and TEM cross-section. Finally, we reported the impact of x-ray acquisition time on the quality and accuracy of the extracted PSD parameters using experimental data and we showed using simulations that a complete PSD extraction can be performed.

SAXS in transmission configuration continue to be improved and shows again very promising result for global shape extraction and line roughness determination; furthermore,

associated data analysis software is becoming very reliable.

#### ACKNOWLEDGMENTS

This research used the Soft Matter Interfaces Beamline (SMI, Beamline 12-ID) of the National Synchrotron Light Source II, a U.S. Department of Energy (DOE) Office of Science User Facility operated for the DOE Office of Science by Brookhaven National Laboratory under Contract No. DE-SC0012704.. Moreover, the Silicon Technologies Division (CEA-LETI) is gratefully acknowledged, for sample manufacturing and provision especially G. Rademaker.

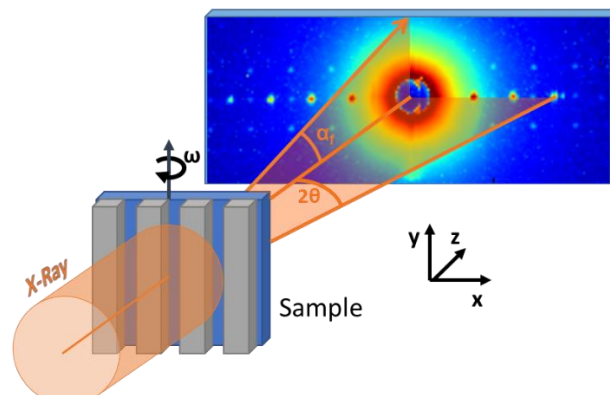


Fig. 1 : CD-SAXS configuration with the x-ray beam propagating along the z axis and the sample rotated along the line direction, i.e. the y axis.

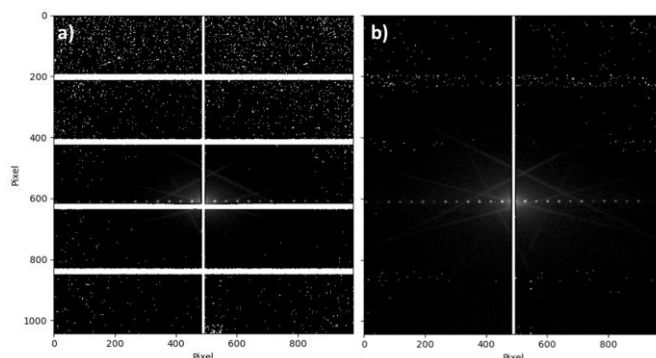


Fig. 2 : Diffraction pattern a) obtained at one position of the detector, with detector gaps visible b) with the combination of two images collected at two different detector positions, to correct for the vertical gaps.

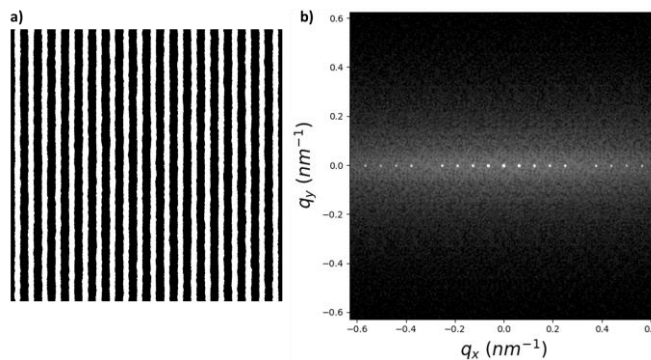


Fig. 3 : a) Virtual sample with roughness induced, b) diffraction pattern simulated with this sample.

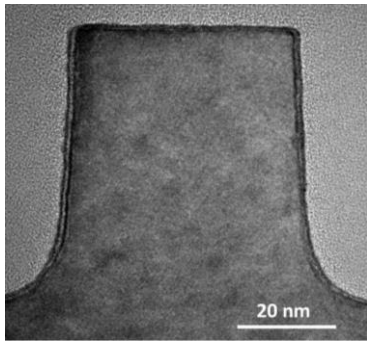


Fig. 4 : TEM cross section of one measure sample "1-113-G"

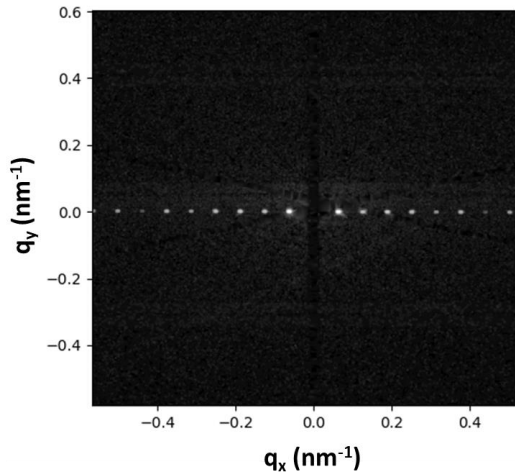


Fig. 5 :  $(q_x, q_y)$  reciprocal space map of the line gratings measure at  $\omega=0^\circ$  for sample "1-113-G".

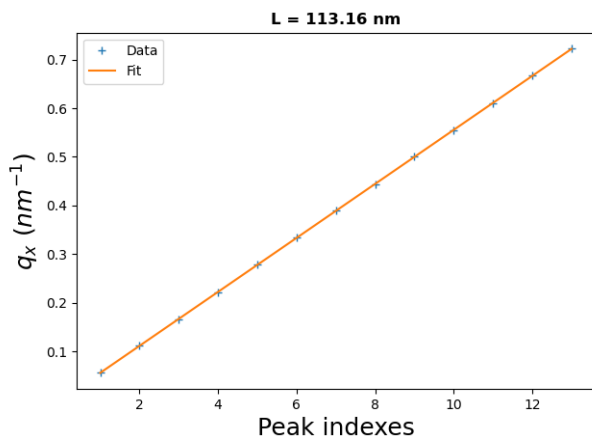


Fig. 6 : Position of Bragg peaks along  $q_x$  as function of peak indexes (blue points) of sample "1-113-G", and the linear fit obtained (orange curve) for an extracted pitch equal to 113.16 nm

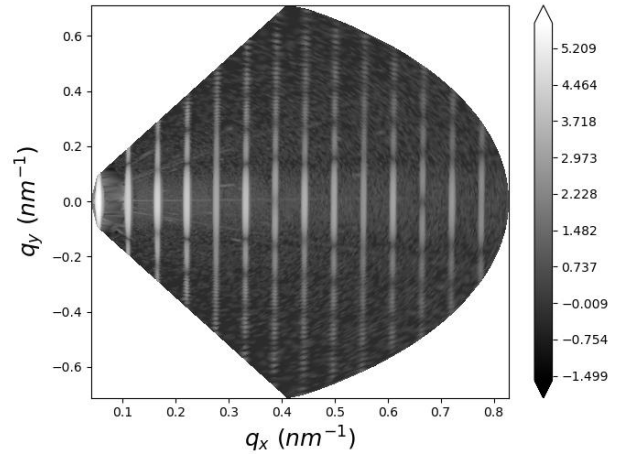


Fig. 7 :  $(q_x, q_z)$  map of line gratings obtained with a sample rotation  $\omega$  from  $-60$  to  $60^\circ$  with a  $1^\circ$  step, for sample "1-113-G"

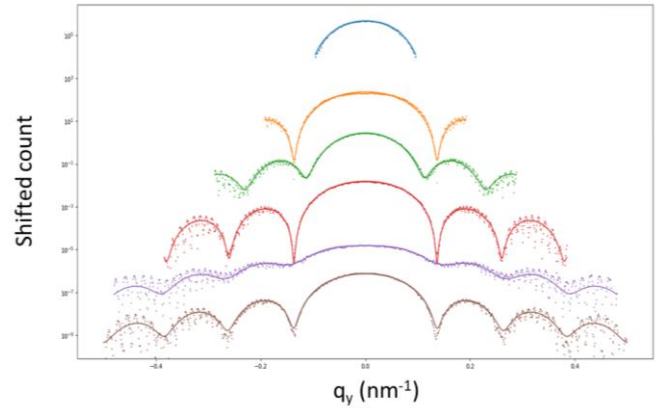


Fig. 8 : Six first peaks intensity extracted (dot) for sample "1-113-G" superpose with eight stacked trapezoids diffraction model (continuis line) after fitting. For the visualisation each peak is shifted on Y axis, top curve correspond to first lattice peak.

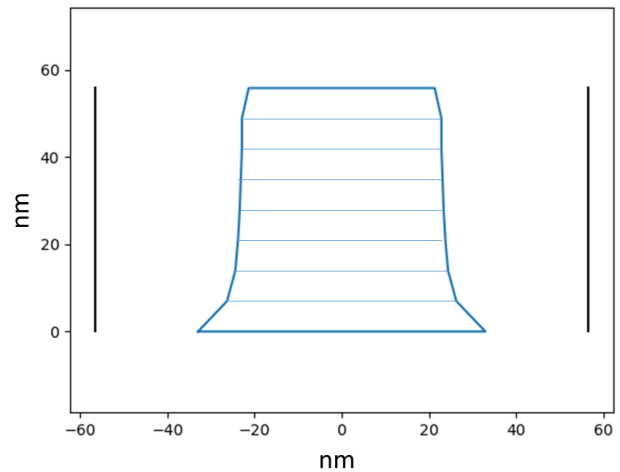


Fig. 9 : Line profil obtained with 8 stacked trapezoids on sample "1-113-G", black line correspond to the pitch distance.

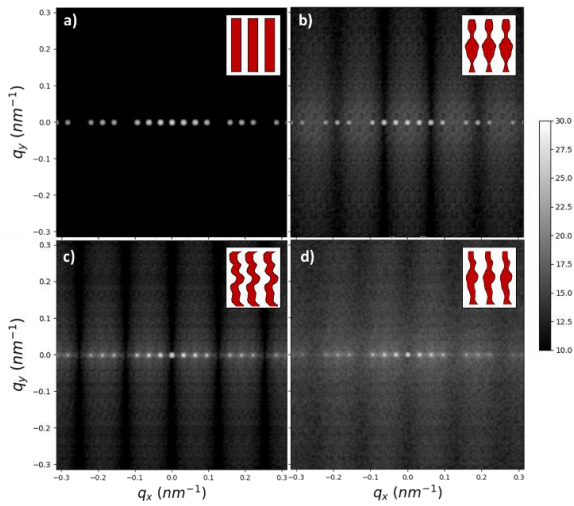


Fig. 10 : Simulations of diffraction patterns for different samples: a) Reference sample (without roughness), b) correlated edges, c) anti-correlated edges and d) uncorrelated edges.

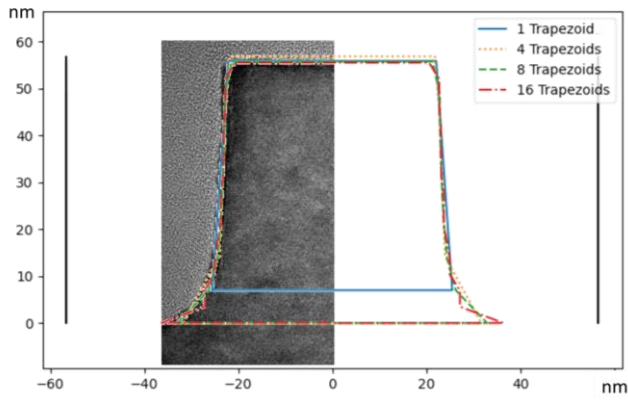


Fig. 11 : In-depth line profiles obtained for stack of trapezoids with a different number of trapezoids  $n$ , superpose with half TEM image for sample "1-113-G".

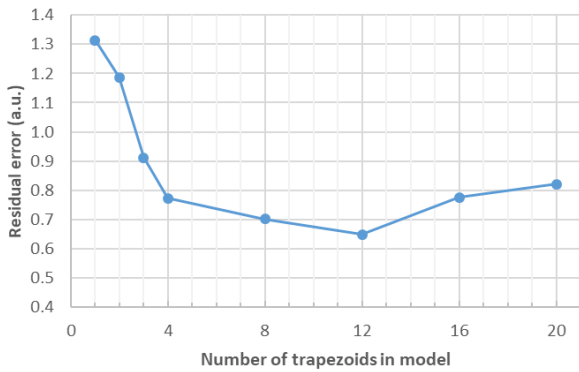


Fig. 12 : Evolution of residual error of the model vs number of trapezoids used. Residual error correspond to difference between experimental data and simulated data corresponding to the best matching profil. Due to the large range between minima and maxima a logarithmic function is used to distribute weight on each data point.

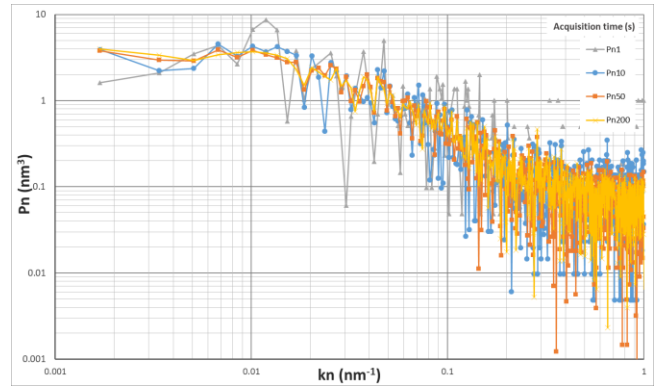


Fig. 13 : Power spectral density extract from the CD-SAXS measurements with different acquisition time. 1 second correspond to 2 acquisitions of 0.5s : 1 top position and 1 bottom position.

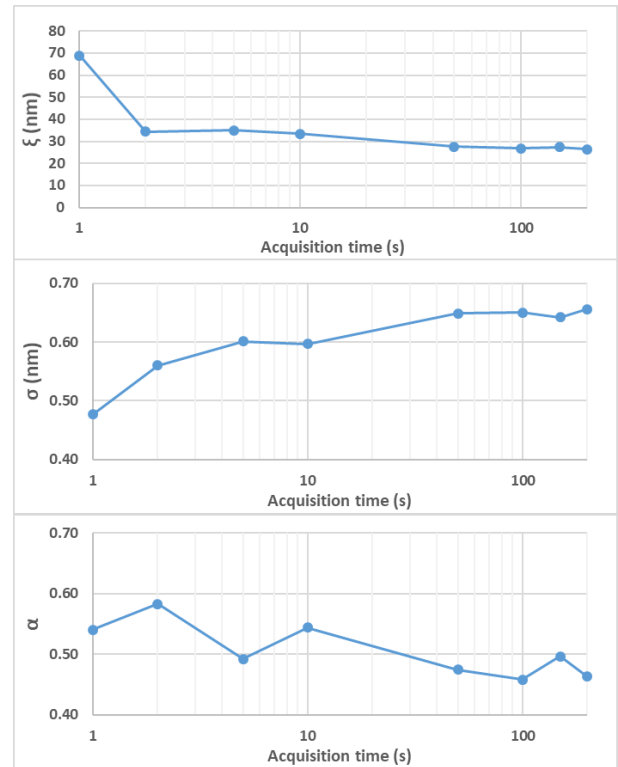


Fig. 14 : Extraction of roughness parameter from PSD fit as a function of diffraction acquisition time.

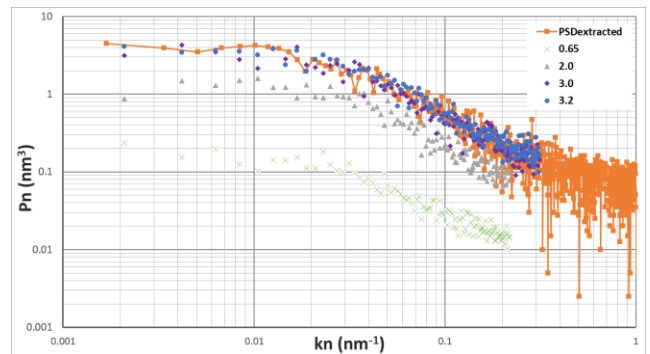


Fig. 15 : Power Spectral Density extracted from experiment (orange line) and the ones obtained from simulation with different value of roughness parameter  $\sigma$ , other roughness parameters  $\alpha$  and  $\xi$  have been respectively set to 0.463 and 26.36 nm

## REFERENCES

- [1] A. Hexemer *et al.*, “A SAXS/WAXS/GISAXS beamline with multilayer monochromator,” in *Journal of Physics: Conference Series*, 2010, vol. 247, p. 012007.
- [2] G. Freychet *et al.*, “Critical-dimension grazing incidence small angle x-ray scattering,” Mar. 2018, p. 37. doi: 10.1117/12.2297518.
- [3] D. F. Sunday, S. List, J. S. Chawla, and R. J. Kline, “Determining the shape and periodicity of nanostructures using small-angle X-ray scattering,” *Journal of Applied Crystallography*, vol. 48, no. 5, pp. 1355–1363, Oct. 2015, doi: 10.1107/S1600576715013369.
- [4] J. Reche, M. Besacier, P. Gergaud, Y. Blancquaert, G. Freychet, and T. Labbaye, “Programmed line width roughness metrology by multitechniques approach,” *Journal of Micro/Nanolithography, MEMS, and MOEMS*, vol. 17, no. 4, p. 041005, 2018.
- [5] J. Reche, M. Besacier, P. Gergaud, and Y. Blancquaert, “Application of PSD for the extraction of programmed line roughness from SAXS,” Mar. 2019, p. 28. doi: 10.1117/12.2514919.
- [6] J. Reche, Y. Blancquaert, G. Freychet, P. Gergaud, and M. Besacier, “Dimensional Control of Line Gratings by Small Angle X-Ray Scattering: Shape and Roughness Extraction,” in *2020 31st Annual SEMI Advanced Semiconductor Manufacturing Conference (ASMC)*, Saratoga Springs, NY, USA, Aug. 2020, pp. 1–6. doi: 10.1109/ASMC49169.2020.9185351.
- [7] B. D. Bunday, M. Bishop, J. S. Villarrubia, and A. E. Vladar, “CD-SEM measurement line-edge roughness test patterns for 193-nm lithography,” in *Metrology, Inspection, and Process Control for Microlithography XVII*, 2003, vol. 5038, pp. 674–688.
- [8] Y. Cohen, B. Yaakovovitz, Y. Tsur, and D. Scheiner, “A novel method for pushing the limits of line edge roughness detection by scatterometry,” Mar. 2008, p. 692220. doi: 10.1117/12.772117.
- [9] C. Wang *et al.*, “Characterization of correlated line edge roughness of nanoscale line gratings using small angle x-ray scattering,” *Journal of Applied Physics*, vol. 102, no. 2, p. 024901, Jul. 2007, doi: 10.1063/1.2753588.
- [10] R. J. Pandolfi *et al.*, “Xi-cam : a versatile interface for data visualization and analysis,” *Journal of Synchrotron Radiation*, vol. 25, no. 4, pp. 1261–1270, Jul. 2018, doi: 10.1107/S1600577518005787.
- [11] C. A. Mack, “Analytic form for the power spectral density in one, two, and three dimensions,” *J. Micro/Nanolith. MEMS MOEMS*, vol. 10, no. 4, p. 040501, Oct. 2011, doi: 10.1117/1.3663567.
- [12] C. Wang, R. L. Jones, E. K. Lin, W.-L. Wu, and J. Leu, “Small angle x-ray scattering measurements of lithographic patterns with sidewall roughness from vertical standing waves,” *Applied Physics Letters*, vol. 90, no. 19, p. 193122, May 2007, doi: 10.1063/1.2737399.
- [13] G. Freychet *et al.*, “Estimation of Line Cross Sections Using Critical-Dimension Grazing-Incidence Small-Angle X-Ray Scattering,” *Physical Review Applied*, vol. 12, no. 4, Oct. 2019, doi: 10.1103/PhysRevApplied.12.044026.
- [14] V. Constantoudis, G. P. Patsis, L. H. A. Leunissen, and E. Gogolides, “Line edge roughness and critical dimension variation: Fractal characterization and comparison using model functions,” *Journal of Vacuum Science & Technology B: Microelectronics and Nanometer Structures*, vol. 22, no. 4, p. 1974, 2004, doi: 10.1116/1.1776561.